



This discussion paper is/has been under review for the journal Atmospheric Chemistry and Physics (ACP). Please refer to the corresponding final paper in ACP if available.

Sunset–sunrise difference in solar occultation ozone measurements (SAGE II, HALOE, and ACE–FTS) and its relationship to tidal vertical winds

T. Sakazaki¹, M. Shiotani¹, M. Suzuki², D. Kinnison³, J. M. Zawodny⁴,
M. McHugh⁵, and K. A. Walker⁶

¹Research Institute for Sustainable Humanosphere, Kyoto University, Uji, Japan

²Institute of Space and Astronautical Science, Japan Aerospace Exploration Agency, Sagamiara, Japan

³National Center for Atmospheric Research, Boulder, USA

⁴NASA Langley Research Center, Hampton, USA

⁵Global Atmospheric Technologies and Sciences, Newport News, USA

⁶Department of Physics, University of Toronto, Toronto, Canada

Received: 9 May 2014 – Accepted: 5 June 2014 – Published: 18 June 2014

Correspondence to: T. Sakazaki (takatoshi_sakazaki@rish.kyoto-u.ac.jp)

Published by Copernicus Publications on behalf of the European Geosciences Union.

Sunset–sunrise difference in solar occultation ozone measurements

T. Sakazaki et al.

Title Page

Abstract

Introduction

Conclusions

References

Tables

Figures



Back

Close

Full Screen / Esc

Printer-friendly Version

Interactive Discussion



Sunset–sunrise difference in solar occultation ozone measurements

T. Sakazaki et al.

Title Page

Abstract

Introduction

Conclusions

References

Tables

Figures



Back

Close

Full Screen / Esc

Printer-friendly Version

Interactive Discussion



measurements (WMO, 2011). Useful datasets for long-term monitoring of vertical profiles of ozone levels can be obtained from solar occultation instruments, such as the Stratospheric Aerosol and Gas Experiment (SAGE) II (McCormick, 1987; McCormick et al., 1989), the Halogen Occultation Experiment (HALOE) (Russell et al., 1993), and the Atmospheric Chemistry Experiment Fourier Transform Spectrometer (ACE-FTS) (Bernath et al., 2005), as they have measurements that are self-calibrating and have high sensitivity. These measurements have been used to detect seasonal and interannual variability, as well as long-term trends, in the stratospheric ozone concentration (e.g., Shiotani and Hasebe, 1994; Randell and Wu, 1996; Newchurch et al., 2003; WMO 2011; Kyrölä et al., 2013).

These solar occultation instruments measure the atmosphere at sunrise and sunset (hereafter SR, SS). It has been reported that there is a difference in the observed values between the SR and SS profiles (hereafter, this is referred to as the sunset–minus–sunrise difference, SSD). For SAGE II, the SSD is reported to be up to 10% between altitudes of 35 and 55 km, with a maximum occurring in the tropics (cf. SAGE II version 5.9 data: Wang et al., 1996; version 6.2 data: McLinden et al., 2009; version 7.0 data: Kyrölä et al., 2013). For HALOE (version 17 data), Brühl et al. (1996) reported an SSD of approximately 5% in the tropical stratopause. SSD values based on ACE–FTS (Fourier Transform Spectrometer) observations have yet to be reported, as far as we know.

Quantification of the SSD and a understanding the source of this difference are necessary for the construction of combined datasets from SR and SS profiles. As we will explore in this study, the SSD could be caused by any one of three factors, including: (1) systematic instrumental/retrieval bias between SR and SS observations; (2) natural diurnal variations; and (3) sampling issues. The factor (3) relates to the fact that if the times of SR and SS measurements are considerably different, the background ozone concentration changes (background changes occur on timescales longer than a day; e.g., subseasonal variations) during such periods are misinterpreted as an example of

SSD (see Sect. 3 for details). In this sense, such spurious contributions, or contamination, should be assessed and removed before discussing the SSD.

In previous studies, the ozone SSD was mainly attributed to factor (1); in other words, factor (2) was thought to be negligible (Wang et al., 1996; Brühl et al., 1996). This was because diurnal variations in stratospheric ozone level were considered to be small and/or to be symmetric between SS and SR, if only photochemistry processes are taken into account. However, note that there are few observations of diurnal variations in the stratosphere and, thus, the above assumption had not been confirmed. In addition, factor (3) may not have been properly considered in some studies (e.g., in the context of interannual variations of the SSD, as shown by Kyrölä et al., 2013; see Sect. 3).

Recently, Sakazaki et al. (2013a; hereafter S13) revealed diurnal variations in ozone concentration from the lower to upper stratosphere using data from both the Superconducting Submillimeter Limb Emission Sounder (SMILES) and chemical-transport models (CTMs). They showed that the peak-to-peak difference in ozone levels reaches 8% during a day. An important point here is that, at some altitudes, the diurnal variations exhibit asymmetric ozone levels when comparing measurements at SS and SR, with the SSD reaching around 4% in the upper stratosphere. S13 showed that the diurnal variations ($[\text{O}_3]'$) are largely controlled by the following equation,

$$\frac{\partial[\text{O}_3]'}{\partial t} = -w' \frac{\partial[\overline{\text{O}_3}]}{\partial z} + S'(1), \quad (1)$$

where t represents time, w' the diurnal variations in the vertical winds (tidal vertical winds), z altitude, $[\overline{\text{O}_3}]$ the daily, zonal mean ozone, and S' the diurnal variations in chemical production or loss. The first term on the right-hand-side denotes the dynamical variation due to vertical transport by atmospheric tidal winds, while the second term denotes the photochemical variation. It should be noted that the dynamical variation results in a maximum at 18:00–20:00 local time (LT) in the upper stratosphere (and at 00:00–06:00 LT in the lower stratosphere; cf. Fig. 7d of S13), possibly causing a positive

Sunset–sunrise
difference in solar
occultation ozone
measurements

T. Sakazaki et al.

Title Page

Abstract

Introduction

Conclusions

References

Tables

Figures



Back

Close

Full Screen / Esc

Printer-friendly Version

Interactive Discussion



Sunset–sunrise difference in solar occultation ozone measurements

T. Sakazaki et al.

Title Page

Abstract

Introduction

Conclusions

References

Tables

Figures



Back

Close

Full Screen / Esc

Printer-friendly Version

Interactive Discussion



dataset covering the full operational periods of each of the three satellite missions. Next, we interpret the SSD in terms of diurnal variations based on SMILES measurements and three-hourly, 3-D-gridded SD–WACCM data, which provide data not only at SR/SS, but for the full diurnal cycle. The 3-D-gridded SD–WACCM data are also used to discuss diurnal variations related to vertical transport and photochemistry. This study focuses on the tropical stratosphere at latitudes of 10° S–10° N between 20 and 60 km in altitude, as the SSD is greatest in the tropics. The remainder of this article is organized as follows. Sections 2 and 3 describe the datasets and analysis methods, respectively. Section 4 describes the SSD and its seasonal variations, and we also discuss the contribution from diurnal ozone variations. Section 5 summarizes our main results.

2 Data description

In this study, the average SSD in the tropical stratosphere within the latitude range 10° S–10° N is analyzed and discussed using data from the three solar occultation instruments: SAGE II, HALOE, and ACE–FTS. To quantify the SSD caused by natural diurnal variations in ozone concentration, data from SMILES limb emission measurements are also analyzed. In addition, two datasets from SD–WACCM are used: the satellite coincidence data subset and the full three-hourly, 3-D-gridded data. The former is used to discuss the difference in SSD among the different satellite datasets, while the latter is used to consider the SSD in terms of diurnal variations. All data are analyzed at geometric altitudes in the stratosphere between 20 and 60 km. Further details are provided in the following subsections.

2.1 SAGE II

The SAGE mission has deployed three instruments; i.e., SAGE I, II, and III. This study uses data from SAGE II because these measurements cover the longest period. SAGE

It was launched in October 1984 on board the Earth Radiation Budget Satellite (ERBS) and remained operational until August 2005, providing data for over 21 years. The ERBS operated in a 610 km altitude, circular orbit with an inclination of 56°. SAGE II is a seven-channel spectrometer capable of obtaining ozone levels from measurements in the 600 nm Chappius band (McCormick et al., 1987, 1989).

Figure 1a shows the SAGE II measurement locations obtained in 1992. The latitude coverage ranges from 80° S to 80° N. SAGE II performed two occultation measurements per orbit, sampling two narrow latitude regions each day. As a result, for each day up to 15 SR and 15 SS profiles were obtained near the same latitude regions, but spaced some 24° apart in longitude. Approximately 10 times per year, the tracks of the SR and SS measurements crossed over. The sampling pattern (i.e., the measurement day of the year at a particular latitude) changed gradually from year to year, and so cover the whole year when data are collected for several years.

We analyzed SAGE II version 7.0 data (Damaedo et al., 2013) obtained during the period 1985–2005. Data were provided for geometric altitudes between 0 and 70 km at intervals of 0.5 km. Geometric altitudes were determined by the viewing geometry with the aid of data from the Modern Era-Retrospective Analysis for Research Applications (MERRA) reanalysis (Rienecker et al., 2011). The uncertainty in altitude registration is less than 20 m (Damaedo et al., 2013). Ozone mixing ratio is calculated as the ratio of ozone number density to atmospheric density, both of which are provided in SAGE II data. The atmospheric density is not measured by SAGE II but derived from MERRA data; however, the results of SSD (%) (cf. Fig. 5b) do not change even if the following analysis is done based on ozone number density. Prior to our detailed analysis, data were screened following the guidelines provided in the SAGE II version 7.0 readme file (https://eosweb.larc.nasa.gov/project/sage2/sage2_release_v7_notes), as follows. Any profile with an error estimate larger than 10% at altitudes between 30 and 50 km was rejected. Data points with an uncertainty estimate of 300% or greater were rejected. Data points at the altitude of and below the occurrence of an aerosol extinction value greater than 0.006 km⁻¹ were rejected. Data points at the altitude of and below

Sunset–sunrise difference in solar occultation ozone measurements

T. Sakazaki et al.

Title Page

Abstract

Introduction

Conclusions

References

Tables

Figures



Back

Close

Full Screen / Esc

Printer-friendly Version

Interactive Discussion



the occurrence of both the 525 nm aerosol extinction value exceeding 0.001 km^{-1} and the 525/1020 extinction ratio of less than 1.4 were rejected. Data points pertaining to altitudes below 35 km with an uncertainty estimate of 200 % (or larger) were rejected. On the basis of this screening process, 3.9 and 5.6 % of all profiles were rejected for the times of SR and SS, respectively.

2.2 HALOE

HALOE was launched in September 1991 on board the Upper Atmosphere Research Satellite (UARS) and remained operational until November 2005, providing data over 15 years. UARS was placed in a 585 km circular orbit, with an inclination of 57° (Russell et al., 1993). Its ozone measurements were made at mid-infrared (mid-IR) wavelengths ($9.6 \mu\text{m}$).

The HALOE measurement locations during 1992 are shown in Fig. 1b. The latitude coverage was approximately 80° S – 80° N . The instruments measured up to 15 SR and 15 SS profiles each day. Approximately 10 times per year, the tracks of the SR and SS measurements crossed over. As with SAGE II, the sampling pattern of HALOE changed gradually from year to year.

We analyzed HALOE version 19 data obtained over the period 1991–2005. Data were provided at 271 pressure levels; i.e., $1000 \times 10^{-(i-1)/30} \text{ hPa}$ ($i = 1, 2, \dots, 271$), between 1000 and 10^{-6} hPa , with a corresponding vertical spacing of approximately 0.5 km. Geometric altitudes were also provided in relation to the pressure levels for each profile, so that we mapped ozone mixing-ratio data onto geometric altitude levels between 0 and 70 km, with a spacing of 0.5 km. No screening was performed on the HALOE data.

HALOE profiles are registered in altitude in an iterative fashion, and the resulting registration is generally assessed to be better than 100 m (McHugh et al., 2003, 2005). Initially, the data are placed on an altitude grid based on the HALOE measurements vs. zenith angle. A first pressure registration is performed using the measured

Sunset–sunrise difference in solar occultation ozone measurements

T. Sakazaki et al.

Title Page

Abstract

Introduction

Conclusions

References

Tables

Figures

◀

▶

◀

▶

Back

Close

Full Screen / Esc

Printer-friendly Version

Interactive Discussion



2.5 SD-WACCM

The NCAR Whole Atmosphere Community Climate Model, version 4 (WACCM4), is a comprehensive numerical model spanning the range of altitude from the Earth's surface to the thermosphere (Garcia et al., 2007; Kinnison et al., 2007; Marsh et al., 2013).

WACCM4 is based on the framework of the NCAR Community Atmosphere Model, version 4 (CAM4), and includes all of the physical parameterizations of CAM4 (Neale et al., 2013) and a finite volume dynamical core (Lin, 2004) for the tracer advection. A version of WACCM4 has been developed that allows the model to be run with specified (external) meteorological fields (Kunz et al., 2011). Here specified dynamics (SD)-WACCM is a chemical transport model (CTM) that uses WACCM4 temperature, horizontal winds, and surface pressure nudged towards MERRA (Rienecker et al., 2011) The CTM data was constrained by meteorological conditions with an hourly timescale, so that they could be directly compared with our observational data. Note that the stratospheric ozone concentration and its diurnal variations in the SD-WACCM data have been analyzed and that the results agreed well with those based on the SMILES data (Imai et al., 2013a; S13).

The horizontal resolution used was 2.5° in longitude and 1.9° in latitude, and the model time step was 30 min. We prepared and analyzed a satellite coincidence data subset, which was sampled at the nearest time and grid point to each satellite measurement. The measurement longitude, latitude, and time were used pertaining to an altitude of 30 km. In other words, we did not consider any altitude dependence of the longitude, latitude, or time for a given profile. This may cause estimation errors in the mesosphere, where the ozone concentration changes rapidly at SR and SS (e.g., S13). Data were provided at 88 pressure levels and mapped onto geometric altitude grids corresponding to those of the satellite datasets. The geometric altitude (z) is calculated

ACPD

14, 16043–16083, 2014

Sunset–sunrise difference in solar occultation ozone measurements

T. Sakazaki et al.

Title Page

Abstract

Introduction

Conclusions

References

Tables

Figures



Back

Close

Full Screen / Esc

Printer-friendly Version

Interactive Discussion



from geopotential height (Z) by the equation,

$$z = \frac{rZ}{\frac{g}{g_0}r - Z}, \quad (2)$$

where g is the gravity at (z, φ) , g_0 ($= 9.80665 \text{ m s}^{-2}$) is the reference gravity, r is the radius of the Earth (cf. Mahoney, 2008, available from the web site http://mtp.mjmahoney.net/www/notes/pt_accuracy/ptaccuracy.html)

As well as the satellite coincidence dataset (only at SR and SS), we analyzed three-hourly, 3-D-gridded data obtained between 2008 and 2010 (hereafter referred to as the “full-grid” data) to extract the full diurnal cycle. We only used data for these three years because of constraints on data storage. As well as ozone mixing ratio, vertical wind in geometric altitude (w) and chemical generation or loss (S) in SD-WACCM data are also analyzed to assess the dynamical and photochemical contributions to the SSD (cf. Eq. 1). On pressure levels, w is calculated on pressure levels from geometric altitude (z) and vertical velocity (ω), by using the formula,

$$w = \frac{Dz}{Dt} = \frac{\partial z}{\partial t} + u \cdot \nabla z + \rho g \omega, \quad (3)$$

where u is horizontal wind, ρ is density, and g is gravity acceleration; then, the calculated w is mapped onto geometric altitude grids.

3 Analysis methods

When calculating the SSD, careful consideration should be given to the sampling issues. Figure 2 shows the number of SR (red) and SS (blue) profiles in the latitude range of 10° S – 10° N obtained during the observation period. We see that the SR and SS profiles are not distributed evenly; e.g., there are no SR (SS) profiles from November to January (May to July) between 2001 and 2005 for SAGE II. This indicates that

Sunset–sunrise difference in solar occultation ozone measurements

T. Sakazaki et al.

Title Page

Abstract

Introduction

Conclusions

References

Tables

Figures



Back

Close

Full Screen / Esc

Printer-friendly Version

Interactive Discussion



Sunset–sunrise difference in solar occultation ozone measurements

T. Sakazaki et al.

Title Page

Abstract

Introduction

Conclusions

References

Tables

Figures

◀

▶

◀

▶

Back

Close

Full Screen / Esc

Printer-friendly Version

Interactive Discussion



measurement days between the SR and SS profiles are less than 10–15 days, seasonal variations still produced significant differences during this period and contaminate the SSD. In fact, this effect is not negligible in the stratosphere, where semiannual variations in ozone concentration associated with the stratospheric semiannual oscillation (SAO) exist (e.g., Ray et al., 1994). Thus, we attempted to further remove the contamination caused by seasonal variations, as follows.

For both SAGE II and HALOE, we assessed the background ozone concentration changes (O_{3_BG}) at each altitude using linear multivariable regression:

$$O_{3_BG} = b + at + q_1 QBO_{10}(t) + q_2 QBO_{30}(t) + \sum_{n=1}^2 (c_n \cos(n\omega t) + s_n \sin(n\omega t)), \quad (4)$$

where t is expressed in days, $QBO_{10}(t)$ and $QBO_{30}(t)$ are the quasi-biennial oscillation (QBO) indices defined by monthly zonal winds at 10 and 30 hPa, respectively, at Singapore (Naujokat, 1986), and $\omega = 2\pi/365.25$ (rad day⁻¹). The QBO indices are used after normalization by one standard deviation and application of a 12 month running mean (e.g., Gebhardt et al., 2013). For the regression, least-squares fitting was applied to the time series of the average of the SR and SS in each pair (i.e., $(SR^i + SS^i)/2$; the time series of open stars in Fig. 3). The resulting O_{3_BG} is also shown in Fig. 3 (solid curve). We see that O_{3_BG} changes by approximately 0.1 ppmv over 10 days, which is comparable with the SSD (see below and Fig. 4).

The SSD caused by seasonal variation for the i th pair (SSD_{seas}^i) was then evaluated as:

$$SSD_{seas}^i = O_{3_BG}(t_{SS}^i) - O_{3_BG}(t_{SR}^i), \quad (5)$$

where t_{SS}^i and t_{SR}^i are the day of i th SS and SR, respectively. Figure 4 also shows SSD_{seas}^i (blue closed circles). SSD_{seas}^i exhibits semiannual variations that follow the ozone SAO, with an amplitude of up to 0.1 ppmv at this altitude. Finally, the corrected

SSD (SSD_{cor}^i ; red open circles in Fig. 4) was calculated as

$$SSD_{cor}^i = SSD_{org}^i - SSD_{seas}^i. \quad (6)$$

We expect that this SSD was only caused by diurnal variations and/or instrumental/retrieval bias.

For ACE–FTS, only four pairs were obtained during the months of interest every year because of the repeating orbit pattern. This leads to incorrect assessment of the seasonal variations (particularly of the SAO) by the above fitting procedure (not shown). Thus, the SSD for ACE (SSD_{cor}^i) was calculated using SSD_{org}^i from ACE–FTS data and SSD_{seas}^i from HALOE data. That is, SSD_{seas}^i is calculated for 2004–2011, using the fitting coefficients estimated from HALOE data during 1990–2005.

Having calculated the SSD for each SR–SS pair, the SSD_{cor}^i was binned and averaged using monthly bins. For example, if the day of a SR–SS pair was 13 April, the relevant SSD_{cor}^i was assigned to the April bin. Figure 4 shows the monthly average values of SSD_{cor}^i , as well as those of SSD_{org}^i and SSD_{seas}^i . If SSD_{org}^i was used for the analysis (see the black curve), it shows a semiannual variation with maxima in February and July/August/September; however, this is partially the result of contamination from SSD_{seas}^i , which shows a semiannual variation (ca. 0.1 ppmv) associated with the stratospheric SAO (see the blue curve; Ray et al., 1994). When this contamination is removed, as is done in the present study, SSD_{cor}^i instead shows an annual variation with a maximum between December and February (see the red curve). This seasonal variation is discussed in Sect. 4.2.

Finally, the annual mean SSD was calculated as the average of the monthly mean SSD_{cor}^i . Note that correction for SSD_{seas}^i is important in the context of the annual mean SSD as well. For SAGE II and HALOE, whose measurements cover the entire year, the annual mean of SSD_{cor}^i is nearly the same as that of SSD_{org}^i , because the annual mean of SSD_{seas}^i should be zero. This is, however, not the case for ACE–FTS, which made tropical measurements only in particular months (i.e., February, April, August, and October). In this case, the annual mean of SSD_{seas}^i is not zero, but reaches a

Sunset–sunrise difference in solar occultation ozone measurements

T. Sakazaki et al.

Title Page

Abstract

Introduction

Conclusions

References

Tables

Figures



Back

Close

Full Screen / Esc

Printer-friendly Version

Interactive Discussion



maximum of approximately 0.1 ppmv; thus, the annual mean of SSD_{org} is not equal to that of SSD_{cor} (not shown).

For SMILES, two kinds of SSDs are calculated with different procedures. The first kind of SSD is based on SR-SS pairs. SR-SS pairs that had more than 10 profiles for both SR and SS were analyzed, and four SR-SS pairs met this requirement (3 November 2009, 31 December 2009, 29 January 2010, and 29 March 2010). Each pair had more than 200 profiles for both SR and SS. In all cases, SR and SS measurements were taken about 5 days apart. Unlike the solar occultation measurements, SMILES observed the $10^{\circ}S-10^{\circ}N$ region almost continuously (see Sect. 2.4). Consequently, the changes in background ozone concentration; i.e., O_{3_BG} in Eq. (4), were defined as the time series of ozone concentration over the region $10^{\circ}S-10^{\circ}N$ to which a five-day running mean was applied. Then, SSD_{seas} was assessed using Eq. (5) and SSD_{cor} was obtained from Eq. (6). The average of the four SSD_{cor} s will be used in Sect. 4.1, while the individual SSD_{cor} s are used in Sect. 4.2 in the context of a discussion of their seasonal dependence. Next, the second kind of SSD is the SSD caused by diurnal variations. This quantity is the difference in ozone levels between 18:00 LT (for SS) and 06:00 LT (for SR), as derived from hourly diurnal ozone-concentration variations in the SMILES data averaged over the period of operation (October 2009–April 2010). The method for extracting hourly diurnal variations from SMILES data was described in S13. Note that the times of SR and SS are 18:00 LT (± 0.3 h) and 06:00 LT (± 0.3 h), respectively, for the region $10^{\circ}S-10^{\circ}N$.

For the SD-WACCM output for satellite coincidences (HALOE, SAGE II, and ACE-FTS), the same method was applied as that used for each satellite dataset. In contrast, for the full-grid SD-WACCM output, diurnal variations as a function of LT were extracted for each latitude and altitude grid point, for each month, as follows. First, three hourly diurnal variations in Universal time (UT) are calculated at each longitude, latitude and altitude grid point. Then, along each latitude band, data at the same local time are averaged to obtain diurnal variations as a function of LT (e.g., 00:00 LT data are the average of (00:00 UT, $0^{\circ}E$), (03:00 UT, $315^{\circ}E$), (06:00 UT, $270^{\circ}E$), (09:00 UT, $225^{\circ}E$),

Sunset–sunrise
difference in solar
occultation ozone
measurements

T. Sakazaki et al.

Title Page

Abstract

Introduction

Conclusions

References

Tables

Figures



Back

Close

Full Screen / Esc

Printer-friendly Version

Interactive Discussion



(12:00 UT, 180° E), (15:00 UT, 135° E), (18:00 UT, 90° E) and (21:00 UT, 45° E)). Using this data, as for SMILES, the SSD caused by diurnal variations, that is, difference between 18:00 and 06:00 LT, was calculated. For SD-WACCM, as was done by S13, the contributions from vertical transport and photochemistry are estimated, by integrating Eq. (1). Diurnal variations of vertical wind (w') and photochemical generation or loss (S') are both derived from the full-grid SD-WACCM output.

4 Results

4.1 Annual mean

Fig. 5a shows the annual mean vertical profiles of the SSD in ozone mixing ratio in the region between 10° S and 10° N, using data from the three solar occultation measurements and from SD-WACCM output during each satellite coincidence. We see that HALOE (blue solid curve) and ACE-FTS (green solid curve) agree well with each other for the entire stratosphere; SD-WACCM results at times of satellite coincidence (blue and green dashed curves) are also quantitatively consistent in the stratosphere (below ~ 55 km). In the lower stratosphere, at an altitude of around 25 km, the SR profiles exhibit 0.05–0.1 ppmv more ozone than the SS profiles. This difference gradually decreases with increasing altitude and reaches zero at about 30 km. In the upper stratosphere, at 40–45 km, the SS profiles exhibit up to 0.2 ppmv more ozone than the SR profiles. Figure 5b shows the ratio of the SSD to the average ozone mixing ratio during the analysis period. The SSD is between –2 and –3% at around 20 km, and gradually increases to 5% at an altitude of 45 km. The SSD near the stratopause is quantitatively consistent with the HALOE result of Brühl et al. (1996), although they only analyzed two latitude bands at around 18° N and 18° S.

SAGE II (red solid curve) shows a similar result to HALOE and ACE-FTS, at least qualitatively, but the SSD in the upper stratosphere is approximately twice as large as those resulting from the other datasets. The SAGE II results are essentially consistent

Sunset–sunrise difference in solar occultation ozone measurements

T. Sakazaki et al.

Title Page

Abstract

Introduction

Conclusions

References

Tables

Figures



Back

Close

Full Screen / Esc

Printer-friendly Version

Interactive Discussion



**Sunset–sunrise
difference in solar
occultation ozone
measurements**

T. Sakazaki et al.

Title Page

Abstract

Introduction

Conclusions

References

Tables

Figures

◀

▶

◀

▶

Back

Close

Full Screen / Esc

Printer-friendly Version

Interactive Discussion



positive-SSD region) and in the lower stratosphere (the negative-SSD region). We conclude that the seasonal dependence of the SSD is mainly caused by that in the diurnal variations in ozone level. Figure 10b shows the seasonal variation of the SSD related to vertical tidal transport only (Eq. 1). Good agreement between Fig. 10a and b again indicates that the SSD can be largely explained by diurnal variations caused by vertical tidal transport. It is also suggested that the seasonal dependence of the SSD is caused by that of the tidal vertical winds.

Although tides are mainly composed of diurnal and semidiurnal components, the former cause the SSD, because the semidiurnal cycle does not cause any difference between two measurements taken 12 h apart (i.e., normal SR and SS at 06:00 and 18:00 LT). Figure 11 shows the tropical month–latitude distributions of the diurnal migrating tide in the vertical winds at 42 and 26 km, derived from the SD–WACCM results. At an altitude of 42 km, the amplitude is greatest during the Northern Hemisphere winter, while a small secondary maximum is discernable in the period August–September between 20 and 10° S. At 26 km, we see similar double maxima, one in February–March and the other in August–September. The seasonal variations in vertical wind are consistent with those in temperature (e.g., Wu et al., 1998; Sakazaki et al., 2012). Sakazaki et al. (2013b) attributed the double maxima to the seasonal dependence of the background zonal winds; the meridional advection of the zonal wind momentum peaks twice a year, producing the tidal seasonal variation in the stratosphere. We conclude that the seasonal variation in the vertical tidal wind causes the variation of the vertical transport of ozone (see Fig. 10b), and, consequently, this results in the seasonal variation of the SSD (see Fig. 10a). The secondary maximum in August–September at an altitude of 42 km, as seen in the vertical wind, does not appear in the SSD, probably because we only analyzed the SSD in the region 10° S–10° N.

locations or times among the datasets. The retrieval procedure in SAGE II has been greatly updated in SAGE II version 7 data (Damadeo et al., 2013). We have so far no clear answer to the difference, and there may be several possibilities as discussed in the following.

5 A SSD could occur if the measurement “altitude” is mistakenly defined at SR and/or SS. But, the observed uncertainty in SSD of $\sim 4\%$ (the difference in SSD between SAGE II and the others at 42 km) corresponds to the uncertainty in altitude of ~ 400 m (at 42 km, the ozone mixing ratio changes 1 % per 100 m in vertical); this seems unrealistic, because an uncertainty of defined altitude is considered 20 m for SAGE II, 100 m
10 for HALOE, and 150 m for ACE-FTS.

Another related issue may be the reproducibility of atmospheric tides in models and reanalyses. We found that the amplitude of diurnal tide in SD-WACCM is up to $\sim 50\%$ smaller in the upper stratosphere than that in data from the Sounding of the Atmosphere using Broadband Emission Radiometry (SABER) measurements (version 2.0
15 data) (not shown). Considering that the SSD is largely attributed to the magnitude of atmospheric tides in vertical wind, it might be possible that the SSD in SD-WACCM data might be underestimated. The weaker tidal signal compared to SABER measurements is also the case for several reanalysis data, as was shown by Sakazaki et al. (2012). Because satellite measurements partly depend on reanalyses in their retrieval processes,
20 the diurnal variations in retrieved ozone amount might be partly biased. For example, the SAGE II retrieval of ozone requires knowledge of the Rayleigh extinction which is related to atmospheric density at the tangent altitude. For version 7.0 data, the MERRA data are used to calculate the Rayleigh extinction. If the MERRA data does not include a realistic diurnal variability in density, the SAGE II ozone SSD will be biased. If, for
25 example, MERRA densities were too large at sunrise and too small at sunset, then the SAGE II ozone would be too small at sunrise and too large at sunset and give rise to a SSD that is too large. Accurate measurements of temperature as well as ozone over a full diurnal cycle would be helpful to resolve this issue.

Sunset–sunrise
difference in solar
occultation ozone
measurements

T. Sakazaki et al.

Title Page

Abstract

Introduction

Conclusions

References

Tables

Figures



Back

Close

Full Screen / Esc

Printer-friendly Version

Interactive Discussion



Sunset–sunrise difference in solar occultation ozone measurements

T. Sakazaki et al.

Title Page

Abstract

Introduction

Conclusions

References

Tables

Figures

◀

▶

◀

▶

Back

Close

Full Screen / Esc

Printer-friendly Version

Interactive Discussion



Acknowledgements. SAGE II data were provided by the NASA Atmospheric Data Center. HALOE data were provided by GATS, Inc., through their Website (<http://haloe.gats-inc.com/home/index.php>). ACE–FTS data were provided by the ACE Science Operations Centre. The Atmospheric Chemistry Experiment (ACE), also known as SCISAT, is a Canadian-led mission mainly supported by the Canadian Space Agency and the Natural Sciences and Engineering Research Council of Canada. SMILES data were provided by the ISAS/JAXA. Monthly zonal wind data from Singapore were obtained from the University of Berlin through its Website (<http://www.geo.fu-berlin.de/en/met/ag/strat/produkte/qbo/index.html>). SABER version 2.0 data were provided by GATS, Inc., through their Website (ftp://saber.gats-inc.com/custom/Temp_O3/). We thank K. Imai for his help in working with the ACE–FTS data. We are also grateful to E. Kyrölä and C. Boone for their helpful suggestions and comments. T. Sakazaki was supported in part by the Japanese Ministry of Education, Culture, Sports, Science and Technology (MEXT), through a Grant-in-Aid for JSPS Fellows (25483400). T. Sakazaki and M. Suzuki were also supported by the International Space Science Institute, Bern, Switzerland (ISSI Team #246, Characterizing Diurnal Variations of Ozone for Improving Ozone Trend Estimates, <http://www.issibern.ch/teams/ozonetrend/>). This study was supported in part by the MEXT through a Grant-in-Aid (25281006), the ISS Science Project Office of ISAS/JAXA, and the Human Spaceflight Mission Directorate of JAXA. All figures were drawn with the GFD–Dennou library.

References

- Beaver, G. M., Gordley, L., and Russell III, J. M.: Halogen Occultation Experiment (HALOE) altitude registration of atmospheric profile measurements: lessons learned and improvements made during the data validation phase, *Proc. SPIE 2266, P. Soc. Photo-Opt. Ins.*, 266–280, doi:10.1117/12.187564, 1994.
- Bernath, P. F., McElroy, C. T., Abrams, M. C., Boone, C. D., Butler, M., Camy-Peyret, C., Carleer, M., Clerbaux, C., Coheur, P.-F., Colin, R., DeCola, P., DeMazière, M., Drummond, J. R., Dufour, D., Evans, W. F. J., Fast, H., Fussen, D., Gilbert, K., Jennings, D. E., Llewellyn, E. J., Lowe, R. P., Mahieu, E., McConnell, J. C., McHugh, M., McLeod, S. D., Michaud, R., Midwinter, C., Nassar, R., Nichitiu, F., Nowlan, C., Rinsland, C. P., Rochon, Y. J., Rowlands, N., Semeniuk, K., Simon, P., Skelton, R., Sloan, J. J., Soucy, M.-A., Strong, K., Tremblay,

Sunset–sunrise difference in solar occultation ozone measurements

T. Sakazaki et al.

Title Page

Abstract

Introduction

Conclusions

References

Tables

Figures



Back

Close

Full Screen / Esc

Printer-friendly Version

Interactive Discussion

P., Turnbull, D., Walker, K. A., Walkty, I., Wardle, D. A., Wehrle, V., Zander, R., and Zou, J.: Atmospheric Chemistry Experiment (ACE): mission overview, *Geophys. Res. Lett.*, 32, L15S01, doi:10.1029/2005GL022386, 2005.

Boone, C. D., Nassar, R., Walker, K. A., Rochon, Y., McLeod, S. D., Rinsland, C. P., and Bernath, P. F.: retrievals for the atmospheric chemistry experiment Fourier-transform spectrometer, *Appl. Optics*, 44, 7218–7231, 2005.

Brühl, C., Drayson, S. R., Russell III, J. M., Crutzen, P. J., McLInerney, J. M., Purcell, P. N., Claude, H., Gernandt, H., McGee, T. J., McDermid, I. S., and Gunson, M. R.: Halogen Occultation Experiment ozone channel validation, *J. Geophys. Res.*, 101, 10,217–10,240, 1996.

Damadeo, R. P., Zawodny, J. M., Thomason, L. W., and Iyer, N.: SAGE version 7.0 algorithm: application to SAGE II, *Atmos. Meas. Tech.*, 6, 3539–3561, doi:10.5194/amt-6-3539-2013, 2013.

Dupuy, E., Walker, K. A., Kar, J., Boone, C. D., McElroy, C. T., Bernath, P. F., Drummond, J. R., Skelton, R., McLeod, S. D., Hughes, R. C., Nowlan, C. R., Dufour, D. G., Zou, J., Nichitiu, F., Strong, K., Baron, P., Bevilacqua, R. M., Blumenstock, T., Bodeker, G. E., Borsdorff, T., Bourassa, A. E., Bovensmann, H., Boyd, I. S., Bracher, A., Brogniez, C., Burrows, J. P., Catoire, V., Ceccherini, S., Chabrillat, S., Christensen, T., Coffey, M. T., Cortesi, U., Davies, J., De Clercq, C., Degenstein, D. A., De Mazière, M., Demoulin, P., Dodion, J., Firanski, B., Fischer, H., Forbes, G., Froidevaux, L., Fussen, D., Gerard, P., Godin-Beekmann, S., Goutail, F., Granville, J., Griffith, D., Haley, C. S., Hannigan, J. W., Höpfner, M., Jin, J. J., Jones, A., Jones, N. B., Jucks, K., Kagawa, A., Kasai, Y., Kerzenmacher, T. E., Kleinböhl, A., Klekociuk, A. R., Kramer, I., Küllmann, H., Kuttippurath, J., Kyrölä, E., Lambert, J.-C., Livesey, N. J., Llewellyn, E. J., Lloyd, N. D., Mahieu, E., Manney, G. L., Marshall, B. T., McConnell, J. C., McCormick, M. P., McDermid, I. S., McHugh, M., McLinden, C. A., Mellqvist, J., Mizutani, K., Murayama, Y., Murtagh, D. P., Oelhaf, H., Parrish, A., Petelina, S. V., Piccolo, C., Pommereau, J.-P., Randall, C. E., Robert, C., Roth, C., Schneider, M., Senten, C., Steck, T., Strandberg, A., Strawbridge, K. B., Sussmann, R., Swart, D. P. J., Tarasick, D. W., Taylor, J. R., Tétard, C., Thomason, L. W., Thompson, A. M., Tully, M. B., Urban, J., Vanhellemont, F., Vigouroux, C., von Clarmann, T., von der Gathen, P., von Savigny, C., Waters, J. W., Witte, J. C., Wolff, M., and Zawodny, J. M.: Validation of ozone measurements from the Atmospheric Chemistry Experiment (ACE), *Atmos. Chem. Phys.*, 9, 287–343, doi:10.5194/acp-9-287-2009, 2009.

**Sunset–sunrise
difference in solar
occultation ozone
measurements**

T. Sakazaki et al.

Title Page

Abstract

Introduction

Conclusions

References

Tables

Figures



Back

Close

Full Screen / Esc

Printer-friendly Version

Interactive Discussion



Garcia, R. R., Marsh, D., Kinnison, D. E., Boville, B., and Sassi, F.: simulations of secular trends in the middle atmosphere, 1950–2003, *J. Geophys. Res.*, 112, D09301, doi:10.1029/2006JD007485, 2007.

Gebhardt, C., Rozanov, A., Hommel, R., Weber, M., Bovensmann, H., Burrows, J. P., Degenstein, D., Froidevaux, L., and Thompson, A. M.: Stratospheric ozone trends and variability as seen by SCIAMACHY from 2002 to 2012, *Atmos. Chem. Phys.*, 14, 831–846, doi:10.5194/acp-14-831-2014, 2014.

Huang, F. T., McPeters, R. D., Bhartia, P. K., Mayr, H. G., Frith, S. M., Russell III, J. M., and Mlynczak, M. G.: temperature diurnal variations (migrating tides) in the stratosphere and lower mesosphere based on measurements from SABER on TIMED, *J. Geophys. Res.*, 115, D16121, doi:10.1029/2009JD013698, 2010.

Imai, K., Manago, N., Mitsuda, C., Naito, Y., Nishimoto, E., Sakazaki, T., Fujiwara, M., Froidevaux, L., von Clarmann, T., Stiller, G. P., Murtagh, D. P., Rong, P., Mlynczak, M. G., Walker, K. A., Kinnison, D. E., Akiyoshi, H., Nakamura, T., Miyasaka, T., Nishibori, T., Mizobuchi, S., Kikuchi, K., Ozeki, H., Takahashi, C., Hayashi, H., Sano, T., Suzuki, M., Takayanagi, M., and Shiotani, M.: Validation of ozone data from the Superconducting Submillimeter-Wave Limb-Emission Sounder (SMILES), *J. Geophys. Res. Atmos.*, 118, 5750–5769, doi:10.1002/jgrd.50434, 2013a.

Imai, K., Fujiwara, M., Inai, Y., Manago, N., Suzuki, M., Sano, T., Mitsuda, C., Naito, Y., Hasebe, F., Koide, T., and Shiotani, M.: Comparison of ozone profiles between Superconducting Submillimeter-Wave Limb-Emission Sounder and worldwide ozonesonde measurements, *J. Geophys. Res. Atmos.*, 118, 12755–12765, doi:10.1002/2013JD021094, 2013b.

Kalnay, E., Kanamitsu, M., Kistler, R., Collins, W., Deaven, D., Gandin, L., Iredell, M., Saha, S., White, G., Woollen, J., Zhu, Y., Chelliah, M., Ebisuzaki, W., W. Higgins, Janowiak, J., Mo, K. C., Ropelewski, C., Wang, J., Leetmaa, A., Reynolds, R., Jenne, R., and Joseph, D.: The NCEP/NCAR 40-year reanalysis project, *B. Am. Meteorol. Soc.*, 77, 437–471, 1996.

Kikuchi, K., Nishibori, T., Ochiai, S., Ozeki, H., Irimajiri, Y., Kasai, Y., Koike, M., Manabe, T., Mizukoshi, K., Murayama, Y., Nagahama, T., Sano, T., Sato, R., Seta, M., Takahashi, C., Takayanagi, M., Masuko, H., Inatani, J., Suzuki, M., and Shiotani, M.: Overview and early results of the Superconducting Submillimeter-Wave Limb-Emission Sounder (SMILES), *J. Geophys. Res.*, 115, D23306, doi:10.1029/2010JD014379, 2010.

Kinnison, D. E., Brasseur, G. P., Walters, S., Garcia, R. R., Sassi, F., Boville, B. A., Marsh, D., Harvey, L., Randall, C., Randel, W., Lamarque, J. F., Emmons, L. K., Hess, P., Or-

Sunset–sunrise difference in solar occultation ozone measurements

T. Sakazaki et al.

Title Page

Abstract

Introduction

Conclusions

References

Tables

Figures



Back

Close

Full Screen / Esc

Printer-friendly Version

Interactive Discussion



lando, J., Tyndall, J., and Pan, L.: Sensitivity of chemical tracers to meteorological parameters in the MOZART-3 chemical transport model, *J. Geophys. Res.*, 112, D20302, doi:10.1029/2006JD007879, 2007.

Kunz, A., L. L. Pan, P. Konopka, D. E. Kinnison, and Tilmes, S.: Chemical and dynamical discontinuity at the extratropical tropopause based on START08 and WACCM analyses, *J. Geophys. Res.*, 116, D24302, doi:10.1029/2011JD016686, 2011.

Kyrölä, E., Laine, M., Sofieva, V., Tamminen, J., Päivärinta, S.-M., Tukiainen, S., Zawodny, J., and Thomason, L.: Combined SAGE II–GOMOS ozone profile data set for 1984–2011 and trend analysis of the vertical distribution of ozone, *Atmos. Chem. Phys.*, 13, 10645–10658, doi:10.5194/acp-13-10645-2013, 2013.

Lin, S.-J.: A “vertically-Lagrangian” finite-volume dynamical core for global atmospheric models, *Mon. Weather Rev.*, 132, 2293–2307, 2004.

Marsh, R. M. and Russell III, J. M.: A tidal explanation for the sunrise/sunset anomaly in HALOE low-latitude nitric oxide observations, *Geophys. Res. Lett.*, 27, 3197–3200, 2000.

Marsh, D. R., Mills, M. J., Kinnison, D. E., Lamarque, J.-F., Calvo, N., and Polvani, L. M.: Climate change from 1850 to 2005 simulated in CESM1(WACCM), 73727391, *J. Climate*, 26, doi:10.1175/JCLI-D-12-00558.1, 2013.

McCormick, M. P.: SAGE II: an overview, *Adv. Space Res.*, 7, 3219–3226, 1987.

McCormick, M. P., Zawodny, J. M., Veiga, R. E., Larsen, J. C., and Wang, P. H.: An overview of SAGE I and II ozone measurements, *Planet. Space Sci.*, 37, 1567–1586, 1989.

McHugh, M., Hervig, M., Magill, B., Thompson, R. E., Remsberg, E., Wrotny, J., and Russell, J.: Improved mesospheric temperature, water vapor and polar mesospheric cloud extinctions from HALO E. *Geophys. Res. Lett.*, 30, 1440, doi:10.1029/2002GL016859, 2003.

McHugh, M., Magill, B., Walker, K. A., Boone, C. D., Bernath, P. F., and Russell, J. M.: Comparison of atmospheric retrievals from ACE and HALOE, *Geophys. Res. Lett.*, 32, 2005.

McLinden, C. A., Tegtmeier, S., and Fioletov, V.: Technical Note: A SAGE-corrected SBUV zonal-mean ozone data set, *Atmos. Chem. Phys.*, 9, 7963–7972, doi:10.5194/acp-9-7963-2009, 2009.

Naujokat, B.: An Update of the Observed Quasi-Biennial Oscillation of the Stratospheric Winds over the Tropics. *J. Atmos. Sci.*, 43, 1873–1877, 1986.

Neale, R. B., Richter, J., Park, S., Lauritzen, P. H., Vavrus, S. J., Rasch, P. J., and Zhang, M.: The Mean Climate of the Community Atmosphere Model (CAM4) in Forced SST and Fully Coupled Experiments, *J. Climate*, 26, 5150–5168, doi:10.1175/JCLI-D-12-00236.1, 2013.

Sunset–sunrise difference in solar occultation ozone measurements

T. Sakazaki et al.

Title Page

Abstract

Introduction

Conclusions

References

Tables

Figures



Back

Close

Full Screen / Esc

Printer-friendly Version

Interactive Discussion



Newchurch, M. J., Yang, E.-S., Cunnold, D. M., Reinsel, G. C., Zawodny, J. M., and Russell III, J. M.: Evidence for slowdown in stratospheric ozone loss: first stage of ozone recovery, *J. Geophys. Res.*, 108, 4507, doi:10.1029/2003JD003471, 2003.

Pallister, R. C. and Tuck, A. F.: The diurnal variation of ozone in the upper stratosphere as a test of photochemical theory, *Q. J. Roy. Meteor. Soc.*, 109, 271–284, 1983.

Parrish, A., Boyd, I. S., Nedoluha, G. E., Bhartia, P. K., Frith, S. M., Kramarova, N. A., Connor, B. J., Bodeker, G. E., Froidevaux, L., Shiotani, M., and Sakazaki, T.: Diurnal variations of stratospheric ozone measured by ground-based microwave remote sensing at the Mauna Loa NDACC site: measurement validation and GEOSCCM model comparison, *Atmos. Chem. Phys. Discuss.*, 13, 31855–31890, doi:10.5194/acpd-13-31855-2013, 2013.

Randel, W. and Wu, F.: Isolation of the ozone QBO in SAGEII data by singular-value decomposition, *J. Atmos. Sci.*, 53, 2546–2559, 1996.

Ray, E. A. and Holton, J. R.: The tropical semiannual oscillations in temperature and ozone as observed by the MLS, *J. Atmos. Sci.*, 51, 3045–3052, 1994.

Rienecker, M. M., Suarez, M. J., Gelaro, R., Todling, R., Bacmeister, J., Liu, E., Bosilovich, M. G., Schubert, S. D., Takacs, L., Kim, G.-K., Bloom, S., Chen, J., Collins, D., Conaty, A., da Silva, A., Gu, W., Joiner, J., Koster, R. D., Lucchesi, R., Molod, A., Owens, T., Pawson, S., Pegion, P., Redder, C. R., Reichle, R., Robertson, F. R., Ruddick, A. G., Sienkiewicz, M., and Woollen, J.: MERRA: NASA's modern-era retrospective analysis for research and applications, *J. Climate*, 24, 3624–3648, doi:10.1175/JCLI-D-11-00015.1, 2011.

Remsberg, E., Deaver, L., Wells, J., Lingenfelter, G., Bhatt, P., Gordley, L., Thompson, R., McHugh, M., Russell III, J. M., Keckhut, P., and Schmidlin, F.: An assessment of the quality of Halogen Occultation Experiment temperature profiles in the mesosphere based on comparisons with Rayleigh backscatter lidar and inflatable falling sphere measurements, *J. Geophys. Res. Atmos.*, 107, 4447, doi:10.1029/2001JD001521, 2002.

Russell, III, J. M., Gordley, L. L., Park, J. H., Drayson, S. R., Hesketh, W. D., Cicerone, R. J., Tuck, A. F., Frederick, J. E., Harries, J. E., and Crutzen, P. J.: The halogen occultation experiment, *J. Geophys. Res.*, 98, 10777–10798, 1993.

Sakazaki, T., Fujiwara, M., Zhang, X., Hagan, M. E., and Forbes, J. M.: Diurnal tides from the troposphere to the lower mesosphere as deduced with TIMED/SABER satellite data and six global reanalysis data sets, *J. Geophys. Res.*, 117, D13108, doi:10.1029/2011JD017117, 2012.

Sunset–sunrise difference in solar occultation ozone measurements

T. Sakazaki et al.

Title Page

Abstract

Introduction

Conclusions

References

Tables

Figures

◀

▶

◀

▶

Back

Close

Full Screen / Esc

Printer-friendly Version

Interactive Discussion



- Sakazaki, T., Fujiwara, M., Mitsuda, C., Imai, K., Manago, N., Naito, Y., Nakamura, T., Akiyoshi, H., Kinnison, D., Sano, T., Suzuki, M., and Shiotani, M.: Diurnal ozone variations in the stratosphere revealed in observations from the Superconducting Submillimeter-Wave Limb-Emission Sounder (SMILES) on board the International Space Station (ISS), *J. Geophys. Res. Atmos.*, 118, 2991–3006, doi:10.1002/jgrd.50220, 2013a.
- Sakazaki, T., Fujiwara, M., and Zhang, X.: Interpretation of the vertical structure and seasonal variation of the diurnal migrating tide from the troposphere to the lower mesosphere, *J. Atmos. Sol.-Terr. Phys.*, 105–106, 66–80, 2013b.
- Shiotani, M. and Hasebe, F.: Stratospheric ozone variations in the equatorial region as seen in Stratospheric Aerosol and Gas Experiment data, *J. Geophys. Res.*, 99, 14575–14584, 1994.
- Schanz, A., Hocke, K., and Kämpfer, N.: Daily ozone cycle in the stratosphere: global, regional and seasonal behaviour modelled with the Whole Atmosphere Community Climate Model, *Atmos. Chem. Phys. Discuss.*, 14, 5561–5609, doi:10.5194/acpd-14-5561-2014, 2014.
- Wang, H. J., Cunnold, D. M., and Bao, X.: A critical analysis of Stratospheric Aerosol and Gas Experiment ozone trends, *J. Geophys. Res.*, 101, 12495–12514, 1996.
- Waymark, C., Walker, K., Boone, C., and Bernath, P.: ACE-FTS version 3.0 data set: Validation and data processing update, *Ann. Geophys.-Italy*, 56, doi:10.4401/ag-6339, 2013.
- World Meteorological Organization (WMO): Scientific assessment of ozone depletion: 2010, Report 52, Global Ozone Research and Monitoring Project, Geneva, 2011.
- Wu, D. L., McLandress, C., Read, W. G., Waters, J. W., and Froidevaux, L.: Equatorial diurnal variations observed in UARS Microwave Limb Sounder temperature during 1991–1994 and simulated by the Canadian Middle Atmosphere Model, *J. Geophys. Res.*, 103, 8909–8917, 1998.
- Zeng, Z., Randel, W., Sokolovskiy, S., Deser, C., Kuo, Y.-H., Hagan, M., Du, J., and Ward, W.: Detection of migrating diurnal tide in the tropical upper troposphere and lower stratosphere using the Challenging Minisatellite Payload radio occultation data, *J. Geophys. Res.*, 113, D03102, doi:10.1029/2007JD008725, 2008.

Sunset–sunrise difference in solar occultation ozone measurements

T. Sakazaki et al.

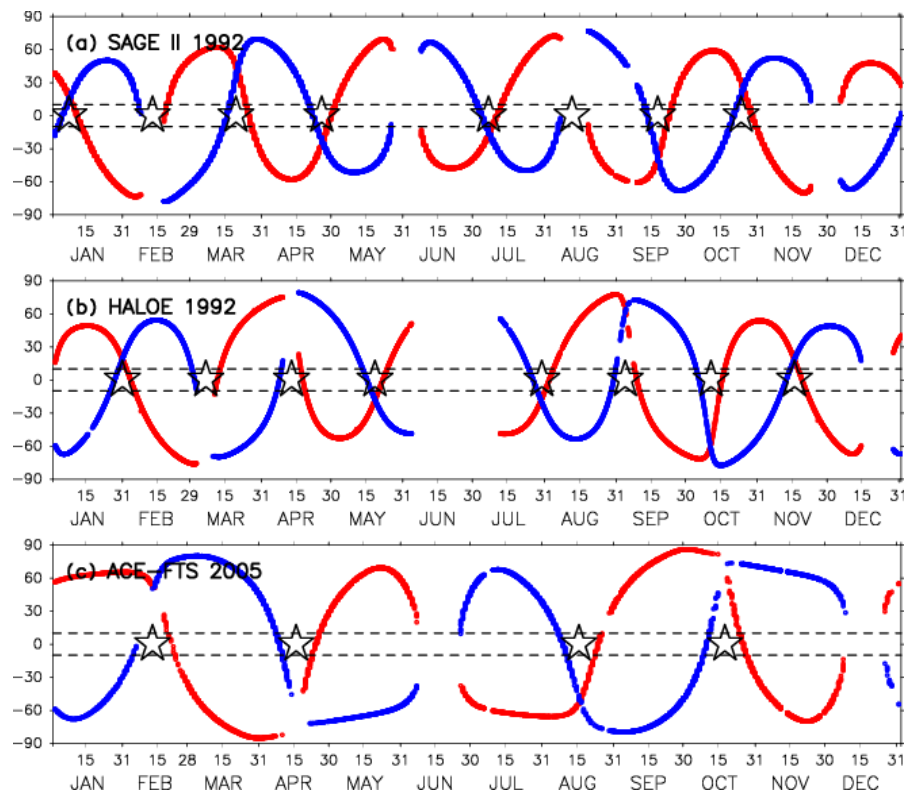


Figure 1. Measurement tracks of (a) SAGE II in 1992, (b) HALOE in 1992, and (c) ACE–FTS in 2005. Red and blue closed circles show SR and SS measurements, respectively. Open stars indicate SR–SS measurement pairs. Dashed lines denote 10° S/N.

Sunset–sunrise
difference in solar
occultation ozone
measurements

T. Sakazaki et al.

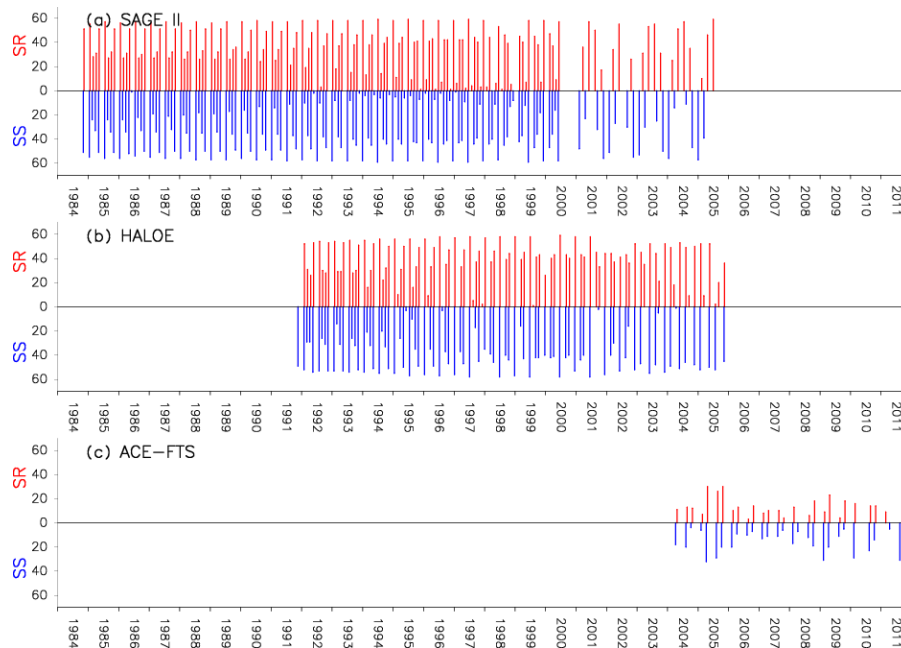


Figure 2. Number of profiles obtained for observations at 10° S–10° N from **(a)** SAGE II, **(b)** HALOE, and **(c)** ACE–FTS. Red and blue bars show the number of SR and SS profiles, respectively.

Title Page

Abstract

Introduction

Conclusions

References

Tables

Figures



Back

Close

Full Screen / Esc

Printer-friendly Version

Interactive Discussion



Sunset–sunrise difference in solar occultation ozone measurements

T. Sakazaki et al.

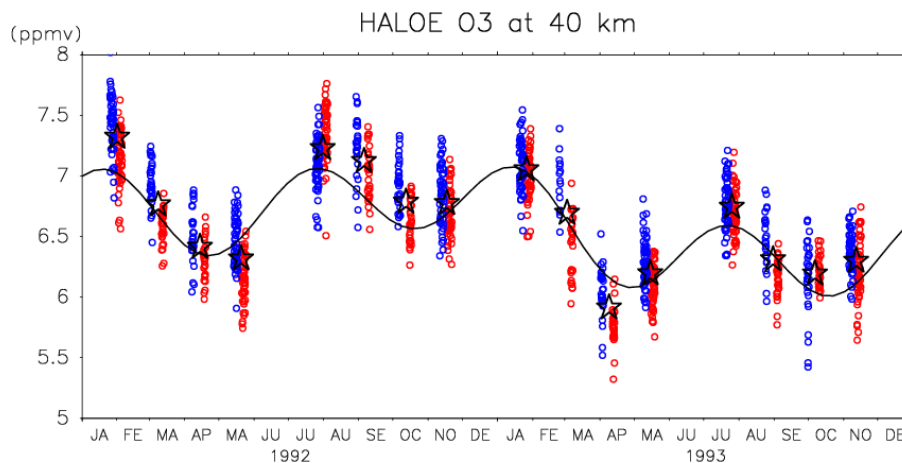


Figure 3. Time series of the ozone mixing ratio observed by HALOE during the period 1992–1993 at an altitude of 40 km (between 10° S and 10° N). Red and blue open circles show individual measurements at SR and SS, respectively. Open stars denote the average values of SR and SS, for each SR–SS pair. The solid curve shows the best-fit function for the average values (see Eq. 4).

[Title Page](#)[Abstract](#)[Introduction](#)[Conclusions](#)[References](#)[Tables](#)[Figures](#)[Back](#)[Close](#)[Full Screen / Esc](#)[Printer-friendly Version](#)[Interactive Discussion](#)

Sunset–sunrise difference in solar occultation ozone measurements

T. Sakazaki et al.

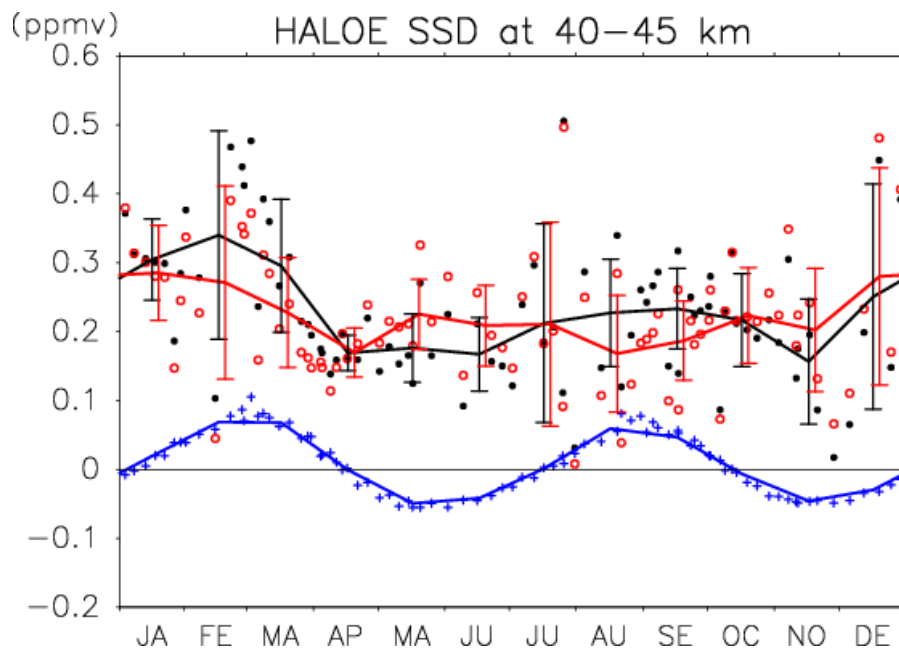


Figure 4. SSD_{org}^i (black closed circles), SSD_{seas}^i (blue crosses), and SSD_{cor}^i (red open circles) averaged at an altitude of 40–45 km for individual SR–SS pairs sorted by time of year, derived from HALOE data during the period 1990–2005. Black, blue, and red curves denote monthly averaged SSD_{org} , SSD_{seas} , and SSD_{cor} , respectively. Vertical bars show one standard deviation for the monthly SSD_{org} and SSD_{cor} .

Title Page

Abstract

Introduction

Conclusions

References

Tables

Figures



Back

Close

Full Screen / Esc

Printer-friendly Version

Interactive Discussion



Sunset–sunrise difference in solar occultation ozone measurements

T. Sakazaki et al.

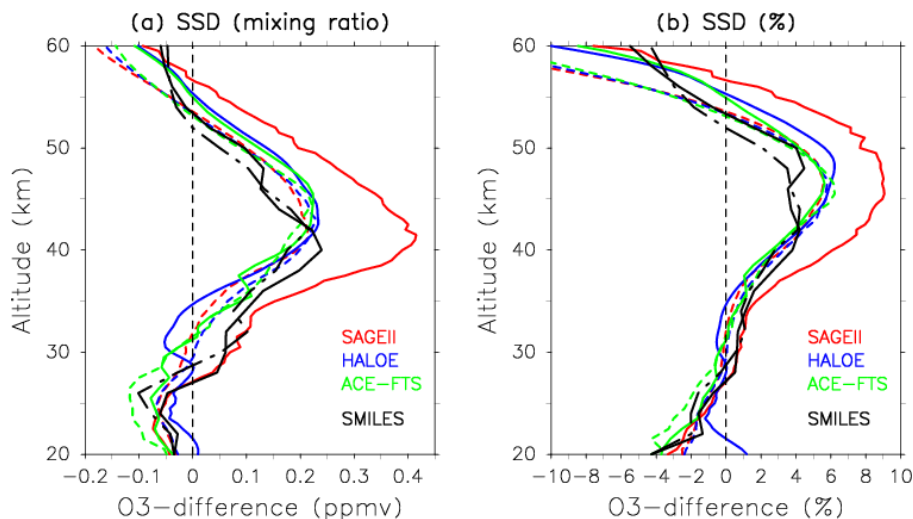


Figure 5. SSD for 10° S–10° N in **(a)** ozone mixing ratio (ppmv), and **(b)** SSD ratio to the daily mean (%), derived from SAGE II (red solid curves), HALOE (blue solid curves), and ACE-FTS (green solid curves). Red, blue, and green dashed curves denote SD-WACCM results at SAGE II, HALOE, and ACE-FTS coincidence, respectively. Black solid curves show the SMILES result (SR and SS are defined by those profiles with a solar zenith angle between 80° and 100°). Black dot-dashed curves show the difference between 18:00 and 06:00 LT, calculated using SMILES data and based on 1 hourly diurnal variations.

Sunset–sunrise
difference in solar
occultation ozone
measurements

T. Sakazaki et al.

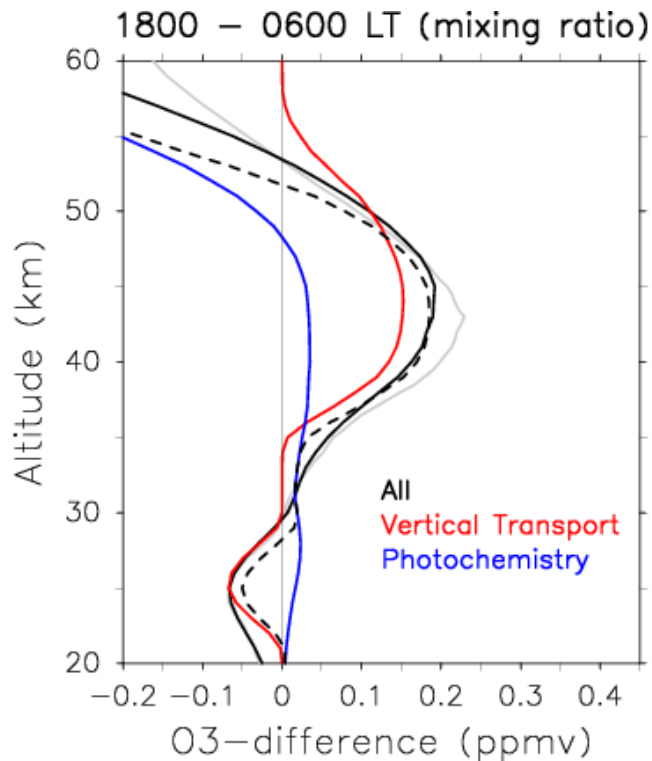


Figure 6. As Fig. 5a, but for the difference between 18:00 and 06:00 LT, as deduced from diurnal variations in ozone concentration based on full-grid SD-WACCM between 2008 and 2010. Solid curve is for the diurnal variations, red solid curve is for the contribution from the vertical transport, blue solid curve is for the contribution from photochemical processes, and the dashed solid curve is for the sum of tidal vertical transport and photochemical processes (see Eq. 1 and Sect. 3 for details). Solid gray curve shows the SSD in SD-WACCM data at HALOE measurement locations (the same as blue dashed curve in Fig. 5) for a reference.

Sunset–sunrise difference in solar occultation ozone measurements

T. Sakazaki et al.

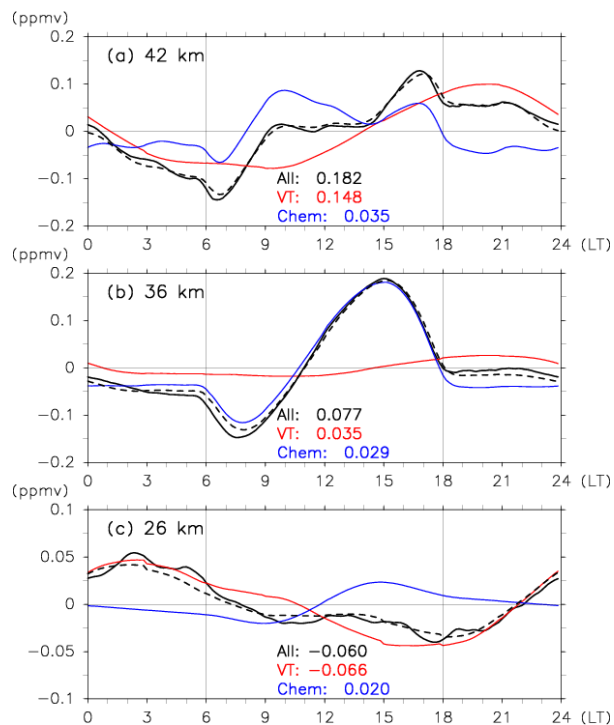


Figure 7. Annual mean diurnal variations in ozone mixing ratio averaged over 10°S – 10°N at altitudes of **(a)** 42 km, **(b)** 36 km, and **(c)** 26 km. Black solid curves are SD-WACCM. Red solid curves show the contribution from tidal vertical transport, and blue solid curves show the contribution from photochemical processes (see Eq. 1 and Sect. 3), while black dashed curves show the sum of the two processes. SR and SS are denoted by thin black solid lines at 06:00 LT and 18:00 LT, respectively. The differences between 18:00 and 06:00 LT in ozone concentration (ppmv) from diurnal variations (“All”), tidal vertical transport (“VT”), and photochemical processes (“Chem”), are shown in each panel.

Sunset–sunrise difference in solar occultation ozone measurements

T. Sakazaki et al.

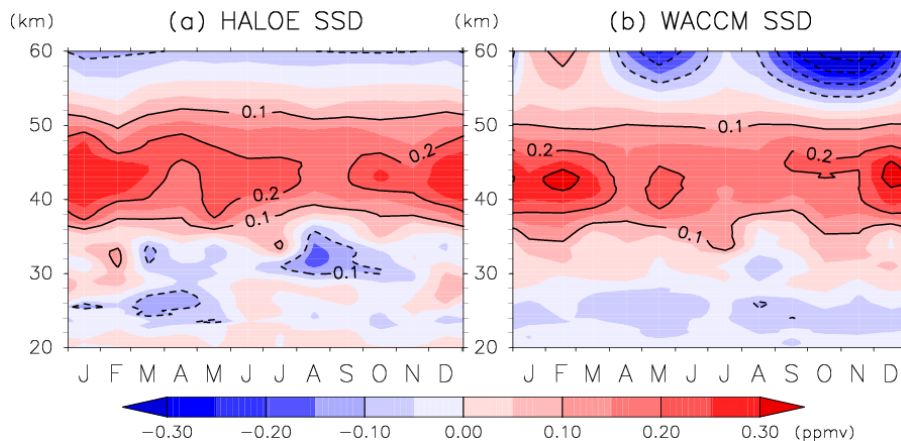


Figure 8. Month–altitude distributions of the SSD for the latitude range 10° S– 10° N, derived from **(a)** HALOE and **(b)** SD–WACCM at HALOE measurement locations. Contour intervals are 0.1 ppmv.

[Title Page](#)[Abstract](#)[Introduction](#)[Conclusions](#)[References](#)[Tables](#)[Figures](#)[◀](#)[▶](#)[◀](#)[▶](#)[Back](#)[Close](#)[Full Screen / Esc](#)[Printer-friendly Version](#)[Interactive Discussion](#)

Sunset–sunrise difference in solar occultation ozone measurements

T. Sakazaki et al.

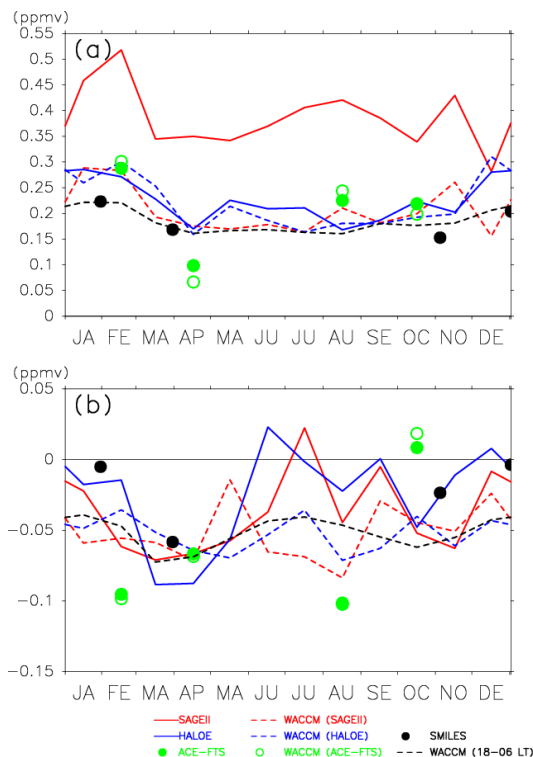


Figure 9. Seasonal variation of O₃ SSD at altitudes of **(a)** 40–45 km and **(b)** 22–28 km, obtained from (red solid curve) SAGE II, (red dashed curve) SD–WACCM at SAGE II locations, (blue solid curve) HALOE, (blue dashed curve) SD–WACCM at HALOE locations, (green closed circles) ACE–FTS, (green open circles) SD–WACCM at ACE–FTS locations, and (black closed circles) SMILES. The black dashed curve shows the difference in ozone between 18:00 and 06:00 LT, as deduced from diurnal variations in ozone concentration based on full-grid SD–WACCM between 2008 and 2010.

Sunset–sunrise difference in solar occultation ozone measurements

T. Sakazaki et al.

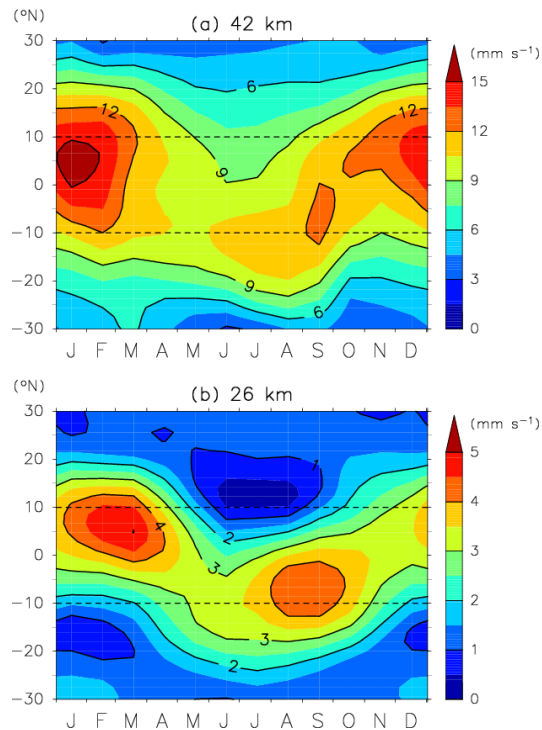


Figure 11. Month–latitude distributions of the amplitude of the diurnal migrating tide in vertical winds at altitudes of **(a)** 42 km and **(b)** 26 km, derived from SD–WACCM data for the period 2008–2010.